Anomalous composition dependence of the superconductivity in In-doped SnTe

Neel Haldolaarachchige, Quinn Gibson, Weiwei Xie, Morten Bormann Nielsen, Satya Kushwaha, and R. J. Cava
Department of Chemistry, Princeton University, Princeton, New Jersey 08544, USA
(Received 24 October 2015; revised manuscript received 4 January 2016; published 26 January 2016)

We report a reinvestigation of superconducting $Sn_{1-x}In_xTe$ at both low and high In doping levels. Considering the system over a broad composition range in a single study allows us to characterize a significant change in the properties as a function of x: The system evolves from a weakly coupled p-type superconductor to a strongly coupled n-type superconductor with increasing indium content. Hall effect measurements show that the carrier density does not vary monotonically with indium content; a change from p-type to n-type is observed near 10% In doping. This is contrary to expectations dictating that In should be a p-type dopant in semiconducting SnTe, because it has one less valance electron than Sn. A crystallographic search for point defects at high x indicates that the material remains ideal NaCl-type over a wide composition range. Density functional theory calculations for In-doped SnTe support a picture where In does not act as a trivial hole dopant but instead forms a distinct, partly filled In 5s-Te 5p hybridized state centered around E_F, which is very different from what is seen for other nominal hole dopants such as Na, Ag, and vacant Sn sites.

DOI: 10.1103/PhysRevB.93.024520

I. INTRODUCTION

SnTe and other II-VI materials with the rock-salt structure type have long attracted attention as models of small band gap semiconductors and have been of renewed recent interest due to the discovery of topological crystalline insulators [1,2]. Hole-doped SnTe is also often considered a model system for superconductivity in a rock-salt type small band gap semiconductor [3–8]. It is known, however, that SnTe shows very different superconducting T_c's when self-hole-doped (i.e., $Sn_{1-\delta}Te$) and chemically doped (i.e., $Sn_{1-x}In_xTe$) to the same hole densities [8–11]. Moreover, indium-doped SnTe maintains the cubic rock-salt structure type up to very high indium contents (about 50%). At such high indium levels, the $Sn_{1-x}In_xTe$ system can no longer be considered as a doped semiconductor, because at such high x, normal charge balance rules based on the number of valence electrons in Sn, In, and Te (i.e., Sn^{2+}, In^{1+}, and Te^{2-}) are strongly violated, i.e., for $Sn_{0.5}In_{0.5}Te$ the In content is an order of magnitude too high for that to be a reasonable model for the system. These observations raise the fundamental question: "What is the nature of indium in $Sn_{1-x}In_xTe$ over a broad composition range?"

Many reports on this materials system postulate that In, with one fewer valence electron than Sn, should be a p-type dopant. This behavior has been well supported experimentally up to about a 9% indium doping level, and a good correlation is found between the chemical In content and the experimentally observed hole carrier densities [11]. It has also been reported that the superconducting T_c of $Sn_{1-x}In_xTe$ continues to increase up to a very high level of doping (50% of In). Although the properties of materials at specific high doping levels have been studied in detail, unlike the case for the lower doping levels, there do not appear to be any reports of a correlation between In content and carrier density in this composition regime; only T_c's and upper critical fields are presented. These considerations therefore raise another question: "Considering what must be an unusual charge state in $Sn_{1-x}In_xTe$ at high In contents, how does the superconducting T_c scale with carrier density at high doping levels, and how are the carrier density and In content related?"

To test these two questions, we have revisited indium-doped SnTe. Our experimental investigations have revealed details of the electronic behavior of the system, leading us to support a picture where indium is not a trivial dopant and to propose that there is a crossover in behavior near 10% In doping. Motivated by the experiments, analysis of our electronic band structure calculations indicates that unlike the case for other monovalent dopants, the In(s) states in $Sn_{1-x}In_xTe$ are prevalent at the Fermi level, supporting a frequently discussed resonant-level-type model [12–14] (along with the analogous Tl-doped PbTe system [15]) in which indium has what is effectively a mixed oxidation state in the system, i.e., that it has partially filled 5s states and thus is formally neither In^{1+} nor In^{3+}. Here we strongly support this viewpoint—we show that superconducting $Sn_{1-x}In_xTe$ cannot be viewed as a simple hole doped semiconductor over the full doping range that leads to superconductivity.

II. EXPERIMENT AND CALCULATION

Polycrystalline samples of $Sn_{1-x}In_xTe$ were prepared by a single step solid state reaction method, starting with ultrahigh purity (5N, 99.999%) elemental Sn, In, and Te. The starting materials were placed in quartz glass tubes and sealed under vacuum. The tubes were heated (180 °C per hour) to 1100 °C and held at that temperature for about five hours. They were then rapidly cooled to 850 °C and held there about 10 hours, after which they were again rapidly cooled to room temperature. The purity and cell parameters of the samples were evaluated by powder x-ray diffraction (PXRD) at room temperature on a Bruker D8 FOCUS diffractometer (CuK_α), and unit cell parameters were determined by least squares fitting of the peak positions with the MAUD program [16]. Further investigation of the sample purity was done with energy dispersive spectroscopy (EDS) by using a FEI XL30 FEG-SEM system equipped with an EVEX EDS. EDS studies on the In-doped samples indicated that the nominal and actual In-doping concentrations are closely matched. Therefore, the nominal concentrations are used throughout this paper. Single crystal x-ray diffraction measurements on a single crystal of

$Sn_{0.6}In_{0.4}Te$ extracted from the characterized polycrystalline sample were carried out at 100 K on a Bruker Apex II diffractometer with Mo radiation. Details of the data collection and analysis are found in the Supplemental Material [17].

The electrical resistivities were measured using a standard four-probe method with an excitation current of 10 mA; small diameter Pt wires were attached to the samples using a conductive epoxy (Epotek H20E). Data were collected from 300–0.4 K in magnetic fields up to 5 T using a Quantum Design physical property measurement system (PPMS) equipped with a ^{3}He cryostat. Hall effect measurements were similarly made with a four-wire configuration geometry, in an applied field of ± 1 T to subtract off the possible longitudinal resistive contribution. Specific heats were measured between 0.4 and 50 K in the PPMS, using a time-relaxation method, at 0 and 5 Tesla applied magnetic fields. The magnetic susceptibilities were measured in a DC field of 10 Oe; the samples were cooled down to 1.8 K in zero-field, the magnetic field was then applied, and the sample magnetization was followed on heating to 6 K [zero-field-cooled (ZFC)], and then on cooling to 1.8 K [field-cooled (FC)] in the PPMS.

The electronic structure calculations were performed by density functional theory (DFT) using the WIEN2K code with a full-potential linearized augmented plane-wave and local orbitals [FP-LAPW + lo] basis [18–21] together with the PBE parametrization [22] of the GGA, with spin orbit coupling (SOC). The plane-wave cutoff parameter $R_{MT}K_{MAX}$ was set to 7 and one hundred k points were used in the Brillouin zone. Supercells were created to accommodate the dopant impurity atoms. The 3% doping level was simulated with a primitive cubic unit cell, and the 12% doping level was simulated with a face centered cubic unit cell, both with one impurity atom per unit cell, placed as a substitution on the Sn site.

III. MATERIALS CHARACTERIZATION

Figure 1 shows the powder x-ray diffraction (PXRD) patterns obtained for the $Sn_{1-x}In_xTe$ materials. The patterns are a good match to the NaCl-type structure of SnTe ($x = 0$, *Fm-3m*, $a = 6.32$ Å), with a composition-dependent unit cell parameter shift. The main panel of Fig. 1 shows that a single phase material with the cubic NaCl structure is maintained in the indium doped samples up to a very high doping level (40%). The upper right inset of Fig. 1 shows an expanded view of the diffraction peak near $2\theta = 40$ degrees. Systematic peak shifts are observed, indicating a systematic shrinking of the unit cell as a function of In content. This behavior is further highlighted by plotting the lattice parameter variation with composition (see lower right inset of Fig. 1), which shows continuous shrinking of the unit cell. A similar shrinkage of the lattice parameter with indium content was found in previous studies of $Sn_{1-x}In_xTe$ up to the 50% doping level [10]. The data support the widely held belief that In systematically replaces the Sn atoms in SnTe to create a single phase NaCl-type structure material. A detailed look at the composition dependence of the lattice parameter variation (see lower right inset of Fig. 1), however, shows that $(\frac{da}{dx})$ changes slope at around the 9% doping level, indicating that there are changes in the system near 9% In content. This apparent structural change around 9–10% indium doping, which has not been previously

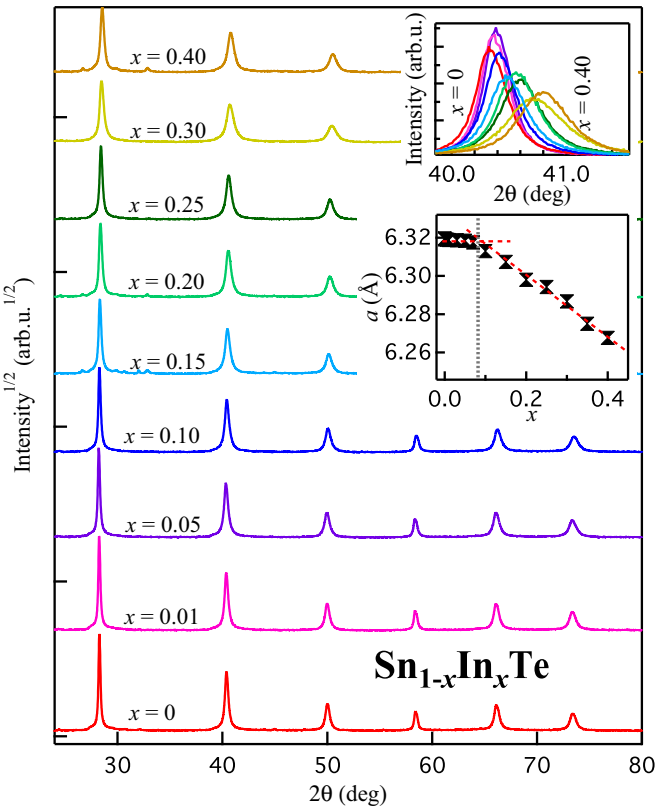

FIG. 1. Powder x-ray diffraction (PXRD) data for the indium doped SnTe. Upper left inset shows systematic peak shift with increasing In doping, and lower left inset shows lattice parameter variation of $Sn_{1-x}In_xTe$ samples in the range of $0 \leqslant x \leqslant 0.4$.

reported, is well correlated with other observations of the electronic properties, as described later in this paper.

Due to the extremely high In content that can be substituted for Sn in SnTe, and the changes in the cell parameter vs composition behavior described above, we considered the possibility that the crystal structure of $Sn_{1-x}In_xTe$ for high x might not be a simple NaCl type. To maintain the charge neutrality expected for semiconductors, for example, a highly defective material of composition $Sn_{1-x}In_xTe_{1-(0.5x)}$ could conceivably be formed at high x. Alternatively, even if the material is essentially stoichiometric at $Sn_{1-x}In_xTe$, at very high x values some or all of the In could be found in tetrahedral interstitial positions in the rocksalt framework, rather than substituting on the octahedral site occupied by Sn; in other words the structural formula could be $[Sn(octahedral)_{1-x}In(tetrahedral)_x]Te$ for high x. Although the $Sn_{1-x}In_xTe$ system has been studied in the past, there appear to be no previous studies specifically focused on looking for these defects. To test these possibilities, we have performed a very careful single crystal structure determination on a single crystal of formula $Sn_{0.6}In_{0.4}Te$ at 100 K. The crystal was found, to high precision, to have the perfect, stoichiometric rocksalt structure with all ideal atomic sites fully occupied and In simply substituting for Sn. Further, there were no displacements of the atomic positions from the high symmetry ideal rocksalt structure positions. Thus our data show that $Sn_{1-x}In_xTe$ at high In content is structurally and chemically exactly as it has been assumed to be in previous studies: Its crystal structure can confidently be assigned

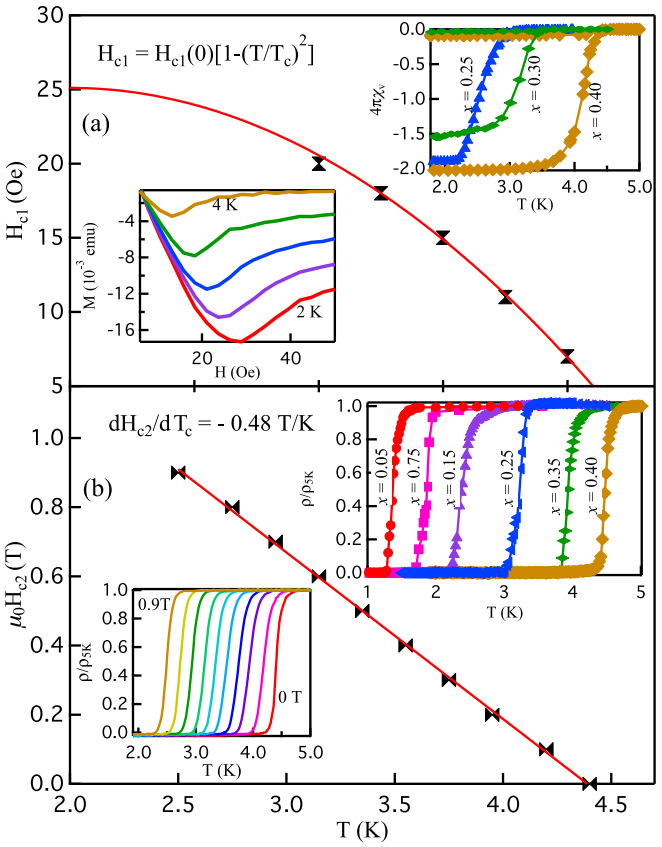

FIG. 2. (a) Lower critical field and (b) upper critical field analysis of 40% Indium doped SnTe sample. The upper left inset of (a) shows the magnetic susceptibility data, and the lower right inset of (a) shows the magnetization as a function of magnetic field at temperatures below the zero field superconducting temperature. The main panel of (a) shows the conventional fitting for determining the lower critical field. The upper inset of (b) shows the resistivity as function doping and shows the resistivity as a function of temperature at different applied magnetic fields.

to a simple, stoichiometric NaCl type. The details of the crystallographic data collection, structural analysis procedure, and refinement results can be found in the Supplemental Material [17].

The upper right inset of Fig. 2(a) shows the magnetic susceptibility characterization of the superconducting transitions of $Sn_{1-x}In_xTe$. The superconducting shielding can be observed in the zero-field-cooled (ZFC-shielding) and field-cooled (FC-Meissner) data. The large volume fractions observed confirm the bulk superconductivity, and a systematic increase of superconducting T_c is easily observed in the high In content range of 20–40%. Very similar superconducting transition temperature values can be observed in both resistivity and magnetization data on the 20–40% indium doped samples. This is a good indication of the homogeneous quality of the polycrystalline samples studied.

The main panel and inset of Fig. 2(a) show the detailed analysis of the lower critical field behavior for $Sn_{0.6}In_{0.4}Te$. The behavior confirms the type-II superconductivity. The solid line in the figure shows the fitting to the conventional formula $H_{c1}(T) = H_{c1}(0)[1-(\frac{T}{T_c})^2]$. The lower critical field can be extracted as $H_{c1}(0) = 21$ Oe [23].

The upper right inset of Fig. 2(b) shows the resistivity variation for $Sn_{1-x}In_xTe$. Pure SnTe shows metalliclike behavior ($\frac{d\rho}{dT} > 0$) with p-type carrier density (10^{20} cm^{-3}) (not shown here), which agrees well with previously published data [9,11]. The material becomes superconducting immediately with small amounts of indium doping; our data are in agreement with the literature. The upper right inset of Fig. 2(b) shows that the superconducting T_c is in the 1–2 K range at low doping levels of indium ($x < 0.1$) and increases linearly with In content. Also, the superconducting T_c increases linearly as a function of doping at higher doping levels ($x > 0.1$). There is a very clear change in the slope of T_c vs x that can be observed at around the 9–10% indium doping level. This behavior is consistent with the observed anomaly in lattice parameter variation shown in Fig. 1 and is possible to observe due to the broad range of compositions studied.

The main panel of Fig. 2(b) shows analysis of the upper critical field of $Sn_{0.6}In_{0.4}Te$. Selecting the 50% normal state resistivity point as the transition temperature, we estimate the orbital upper critical field, $\mu_0 H_{c2}(0)$, from the Werthamer-Helfand-Hohenberg (WHH) expression $\mu_0 H_{c2}(0) = -0.693 T_c \frac{dH_{c2}}{dT}|_{T=T_c}$ [24–27], which agrees well with the reported values for high In content SnTe [28,29]. A linear relationship is observed [Fig. 2(b)] between $\mu_0 H_{c2}$ and T_c. The slope ($\frac{d\mu_0 H_{c2}}{dT_c} = -0.48 T/K$) is used to calculate $\mu_0 H_{c2}(0) = 1.46$ T. $\mu_0 H_{c2}(0)$ can then be used to estimate the coherence length $\xi(0) = \sqrt{\Phi_0/2\pi H_{c2}(0)} = 150$ Å, where $\Phi_0 = \frac{hc}{2e}$ is the magnetic flux quantum [30,31]. From the relation $H_{c1}(0) = \frac{\phi_0}{4\pi\lambda^2} ln \frac{\lambda}{\xi}$, we find the magnetic penetration depth to be $\lambda(0) = 5000$ Å and the Ginzburg-Landau parameter $\kappa = \frac{\lambda}{\xi} = 33$. Using these parameters and the relation $H_{c2}(0)H_{c1}(0) = H_c(0)^2[ln\kappa(0) + 0.08]$, the thermodynamic critical field $H_c(0)$ is found to be 0.85 mT. The superconducting parameters determined here for $Sn_{0.6}In_{0.4}Te$ are summarized in Table I.

TABLE I. Superconducting parameters of the cubic p-type and n-type indium doped SnTe systems.

Parameter	Units	$Sn_{0.95}In_{0.05}Te$	$Sn_{0.6}In_{0.4}Te$
T_c	K	1.18	4.2
$\frac{dH_{c2}}{dT}\|_{T=T_c}$	TK^{-1}		−0.48
$\mu_0 H_{c1}(0)$	Oe		21
$\mu_0 H_{c2}(0)$	T		1.46
$\mu_0 H^{Pauli}$	T	2.23	7.81
$\mu_0 H(0)$	mT		0.85
$\xi(0)$	Å		150.2
$\lambda(0)$	Å		5000
$\kappa(0)$	Å		33.28
$\gamma(0)$	$\frac{mJ}{mol\ K^2}$	0.94	2.47
$\frac{\Delta C}{\gamma T_c}$		1.27	1.98
Θ_D	K	204	162
λ_{ep}		0.52	0.79
$N(E_F)$	$\frac{eV}{f.u.}$	0.44	1.17

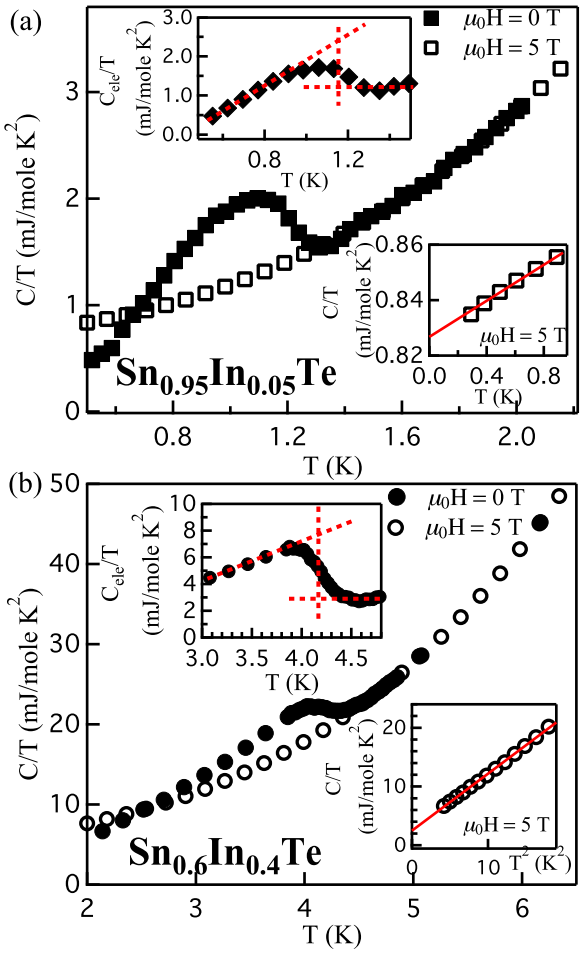

FIG. 3. Heat capacity analysis of (a) 5% and (b) 40% indium doped SnTe samples. The upper left insets of both panels show the superconducting phase transitions in the electronic heat capacity, and the lower right insets show the heat capacity at 5 Tesla applied magnetic field.

Figure 3 shows the analysis of the superconducting transition by specific heat measurements for p-type $Sn_{0.95}In_{0.05}Te$ and n-type $Sn_{0.6}In_{0.4}Te$. The main panel of Fig. 3(a) shows $\frac{C}{T}$ as a function of T for $Sn_{0.95}In_{0.05}Te$, characterizing the specific heat jump at the thermodynamic transition. This jump is completely suppressed under a 5 T applied magnetic field. The superconducting transition temperature $T_c = 1.18$ K is shown in the upper left inset of Fig. 3(a), as extracted by the standard equal area construction method. We find that the low temperature normal state specific heat can be well fitted with $\frac{C}{T} = \gamma_n + \beta T^2$, where $\gamma_n T$ represents the electronic contribution in the normal state, and βT^3 describe the lattice-phonon contributions to the specific heat. The solid line in the lower right inset in Fig. 3(a) shows the fitting; the electronic specific heat coefficient $\gamma_n = 0.82 \frac{mJ}{\text{mol } K^2}$ and the phonon contribution $\beta = 0.45 \frac{mJ}{\text{mol } K^3}$ are extracted from the fit, consistent with the previously reported values [9,11].

The main panel of Fig. 3(b) shows $\frac{C}{T}$ as a function of T for $Sn_{0.6}In_{0.4}Te$. The specific heat jump is completely suppressed under a 5 T applied magnetic field. The superconducting transition temperature $T_c = 4.2$ K is shown in the upper left inset of Fig. 3(b), as extracted by the standard equal area construction method. Again, the low temperature normal state specific heat can be well fitted with $\frac{C}{T} = \gamma_n + \beta T^2$. The solid line in the lower right inset in Fig. 3(b) shows the fitting; the electronic specific heat coefficient $\gamma_n = 2.47 \frac{mJ}{\text{mol } K^2}$ and the phonon contribution $\beta = 0.97 \frac{mJ}{\text{mol } K^3}$ are extracted from the fit. The value of γ_n for this highly In-doped n-type superconductor is much higher than that of the low level indium doped p-type sample. The specific heat data are a clear indication that a significant difference is present between the low and high level indium doped samples.

The ratio $\frac{\Delta C}{\gamma T_c}$ can be used to measure the strength of the electron-phonon coupling [32]. The specific heat jump $\frac{\Delta C}{T_c}$ for $Sn_{0.95}In_{0.05}Te$ is about 1.2 $\frac{mJ}{\text{mol } K^2}$, which results in the value of $\frac{\Delta C}{\gamma T_c}$ of 1.27. This value is about the same as the BCS prediction for weakly electron-phonon coupled superconductors and also agrees with previously reported values of low level of indium doped samples [9,11]. However, the specific heat jump $\frac{\Delta C}{T_c}$ for the sample of $Sn_{0.6}In_{0.4}Te$ is about 4.9 $\frac{mJ}{\text{mol } K^2}$, which results in a value of $\frac{\Delta C}{\gamma T_c}$ of 1.98. This is higher than that of the weak-coupling limit for conventional BCS superconductors. Therefore, the results suggest that $Sn_{0.6}In_{0.4}Te$ is a strongly electron-phonon coupled superconducting system. The observed values of $\frac{\Delta C}{\gamma T_c}$ show that the low and high doping levels of indium in SnTe make two distinct types of superconductors.

In a simple Debye model for the phonon contribution to the specific heat, the β_1 coefficient is related to the Debye temperature Θ_D through $\beta = nN_A \frac{12}{5}\pi^4 R\Theta_D^{-3}$, where $R = 8.314 \frac{J}{\text{mol } K}$, n is the number of atoms per formula unit, and N_A is Avogadro' s number. The calculated Debye temperatures are thus 204 K and 162 K for 5% and 40% indium doped samples, which are similar to the previously reported values on chemically doped SnTe, PbTe, and related systems [9,15,33]. An estimation of the strength of the electron-phonon coupling can be derived from the McMillan formula $\lambda_{ep} = \frac{1.04+\mu^* ln\frac{\Theta_D}{1.45T_c}}{(1-0.62\mu^*)ln\frac{\Theta_D}{1.45T_c}-1.04}$. The McMillan model contains the dimensionless electron-phonon coupling constant λ_{ep}, which, in the Eliashberg theory, is related to the phonon spectrum and the density of states [34,35]. This parameter λ_{ep} represents the attractive interaction, while the second parameter μ^* accounts for the screened Coulomb repulsion. Using the Debye temperature Θ_D and the critical temperature T_c, and making the common assumption that $\mu^* = 0.15$ [34], the electron-phonon coupling constants (λ_{ep}) are 0.52 and 0.79 for 5% and 40% indium doped samples. Thus, our characterization of the superconducting transitions supports the conclusion that the 5% indium doped sample can be categorized as a weakly coupled superconductor, and the 40% indium doped sample can be categorized as a strongly coupled superconductor.

The value of γ extracted from the measured specific heat data corresponds to a normalized electronic density of states at the Fermi energy N(E_F). The following values for the density of states, 0.44 and 1.17 states/(eV f.u.) (f.u. stands for formula unit) for 5% and 40% indium doped samples are thus estimated from the relation $\gamma = \pi^{3/2} k_B^2 N(E_F)(1 + \lambda_{ep})$. The value of N($E_F$) for the 5% In-doped samples is consistent with previous reports for low In doping levels, but N(E_F) for the 40% doped sample is much higher, consistent with the fact that higher In

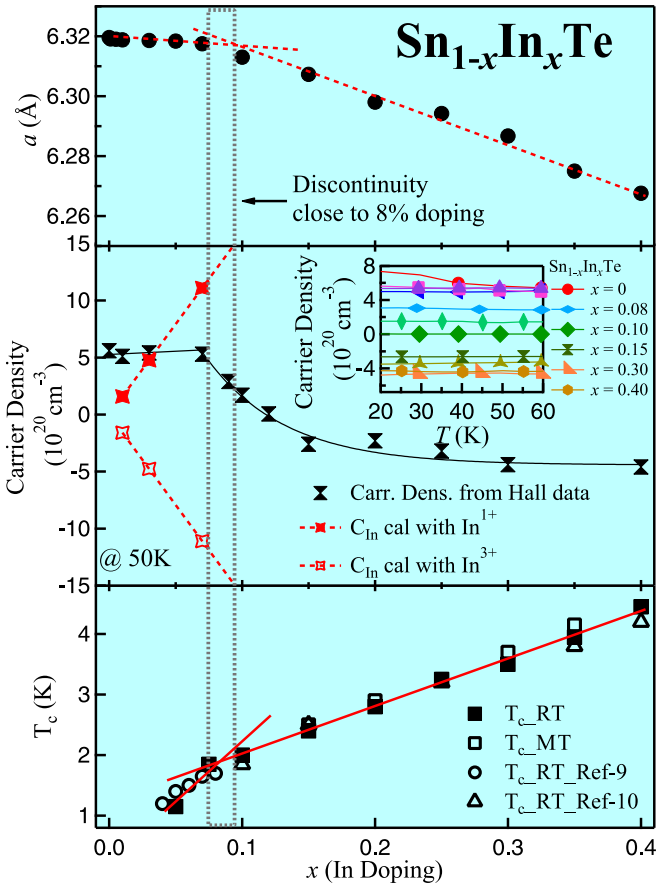

FIG. 4. The (a) lattice parameter variation, (b) carrier density variation and volume density of indium atoms in the doped system, and (c) superconducting transition temperature variation, as a function of fractional indium content in the cubic In-doped SnTe crystal system. The inset of (b) shows the raw data for the carrier density determination at low T. Solid lines in all panels are guides to the eye.

content samples show much higher superconducting T_c's than the lower In content samples.

Figures 4(a)–4(c) are a summary that shows the lattice parameter variation, carrier density variation, and superconducting temperature variation as a function of indium doping in SnTe. It can clearly be seen that there is a change at the 9–10% indium doping level in Fig. 4(a) that is well correlated with the p to n type crossover that is seen in Fig. 4(b). At low doping levels of indium ($x < 10\%$) the system remains p type, which agrees well with previous reports. However, when the doping level goes beyond a critical doping level ($x = 10\%$), the system shows anomalous behavior of the carrier density. At higher doping levels of indium ($x > 10\%$), the system changes to n type, and the composition dependence of the carrier density saturates quickly. This change should be connected to some kind of Fermi surface reconstruction; the behavior is not consistent with a picture of hole doping through In substitution for Sn due to its one fewer electron, a picture which we confirm to be true only up to about 9% indium doping. Figure 4(b) also shows the volume carrier density expected by assuming that every dopant indium atom donates a hole (i.e., if it was formally "In^{1+}"), or an electron (i.e., if it was formally "In^{3+}"), into the SnTe unit cell. In such cases the carrier density as a function of dopant concentration should linearly increase in a positive direction for a formal "In^{1+}" substitution or increase in a negative direction for a formal "In^{3+}" substitution. However, the behavior in this system is much more complicated than that. In doping results in the unexpected suppression of the p-type carrier density at high x and, that at a high doping level, the carrier type changes to n type. More detailed experimental studies of single crystals in this composition regime to characterize this crossover in more detail would be an interesting avenue for future work.

It can be observed that the superconductivity emerges immediately with indium doping into SnTe [Fig. 4(c)]. The superconducting T_c continuously increases as a function of doping. However, there is a clear deviation at 9–10% indium doping level in the rate of increase of the superconducting temperature as a function of doping; $(\frac{dT_c}{dx_{In}})$ is higher at lower doping levels of indium ($x < 0.1$) and becomes smaller when $x > 0.1$. This point of deviation around 10% indium is well correlated with the lattice parameter and carrier density variations.

IV. ELECTRONIC STRUCTURE

Future experimental investigation of the higher In content materials will be of interest, but here we look in more detail at the apparent complexity of the electronic system by performing electronic band structure studies on model materials that simulate the effects of doping in SnTe. In order to theoretically investigate the electronic structure of doped SnTe, DFT calculations were performed on supercells containing different levels of In, Ag, Na, and Sn vacancies; the latter dopants are considered for comparison to the In case. Figure 5 shows the electronic band structure for 3% doped SnTe with In, Ag, Na, and vacancy dopants. Quite dramatically, the Ag, Na, and Sn-vacancy doped models are qualitatively very similar, with the Fermi energy about 200 meV deep in the valence band. However, the model for the In doped material is qualitatively different. The Fermi energy is less deep in the valence band, and there is a distinct in-gap state not seen in the other calculations. The fat bands, which allow the orbital origin of this in-gap state to be determined, show that it is due to the contributions from the In 5s orbital. Further analysis shows this band to be composed primarily of In 5s and Te 5p orbitals. This in-gap band cuts through the Fermi energy at multiple points and thus contributes to the electronic properties of the material. This already indicates an unusual doping mechanism. While In is creating holes in the valence band manifold, it is simultaneously creating other electron and hole pockets through the creation of an impurity band centered around E_F.

This effect is even more pronounced at higher doping levels. Figure 6 shows the electronic structures for In, Ag, Na, and vacancy doped SnTe at 12 percent doping. Here, again, the Na, Ag, and Sn vacancy doped compounds are very similar, whereas the indium doped compound is qualitatively very different. For one, the Fermi energy is considerably deeper in the valence band for the Ag, Na, and defect-doped compounds than for In. Furthermore, the same in-gap state present in the 3 percent doped calculation is present here. Indeed, this band traverses the entire band gap. This compound cannot be considered to be a doped semiconductor, as artificially

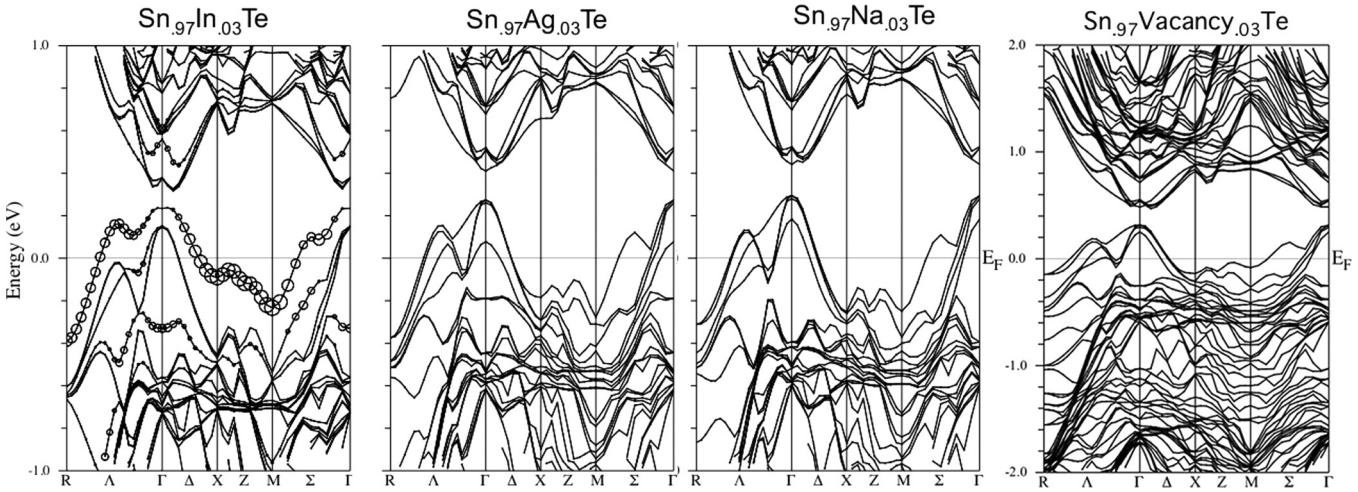

FIG. 5. Calculated electronic band structure for 3% In, Ag, and Na and vacancy doped SnTe. The resonant band at E_F can be observed only in the In doped case.

adding electrons will not bring the Fermi level into a band gap. Finally, the Fermi level is about the same depth in the valence band as is seen for the 3 percent In doping level. While these calculations cannot be directly compared, as the 12 percent and 3 percent calculations needed different unit cell symmetries, this certainly indicates that there is a nonlinear dependence of hole concentration on indium doping level, at least at high doping levels. This is indeed what is observed experimentally. In fact, as the In impurity band is creating its own Fermi surface, at high doping levels, it may not be meaningful to distinguish between different hole concentrations, as the Fermi surface is now more complex than a single pocket. What is striking is that in both cases, the In dopant is creating an impurity band that is relatively well separated from the other bulk bands, and which is also not very dispersive in energy. This is characteristic of a resonant level type dopant, as has been discussed in the thermoelectric and related literature [12–15].

The resonant aspect of this impurity state is also apparent in the density of states. Figure 7 shows the DOS for the In, Ag, and Na doped compounds at both the 3 percent and 12 percent doping levels. Again, near E_F, the Ag and Na samples resemble each other well, while the In one is different. The In doped compound at 3 percent has a small "doublet" peak, which sits right at E_F, that is not present in the others. At 12 percent, this has evolved into a tall, well separated peak that is bisected by the Fermi energy. Further analysis shows that both of these peaks have nontrivial In 5*s* character, along with Te 5*p* character. This indicates that the impurity state that is so important in In doped SnTe appears to come from a hybridization of In 5*s* and Te 5*p* orbitals. Due to the inert pair effect, it is very unusual to have 5*s* or 6*s* states at the Fermi level (indeed, in SnTe the Sn 5*s* states appear about 5 eV below E_F); some well-known compounds that do, such as K doped $BaBiO_3$, exhibit superconductivity [36]. It is therefore very likely that the hybrid state created by the In 5*s* and Te 5*p* orbitals plays a significant role in the superconductivity. This would explain why In doped SnTe exhibits an order of magnitude higher T_c than self-doped SnTe, even at the same nominal hole concentration. Further calculations indicate that

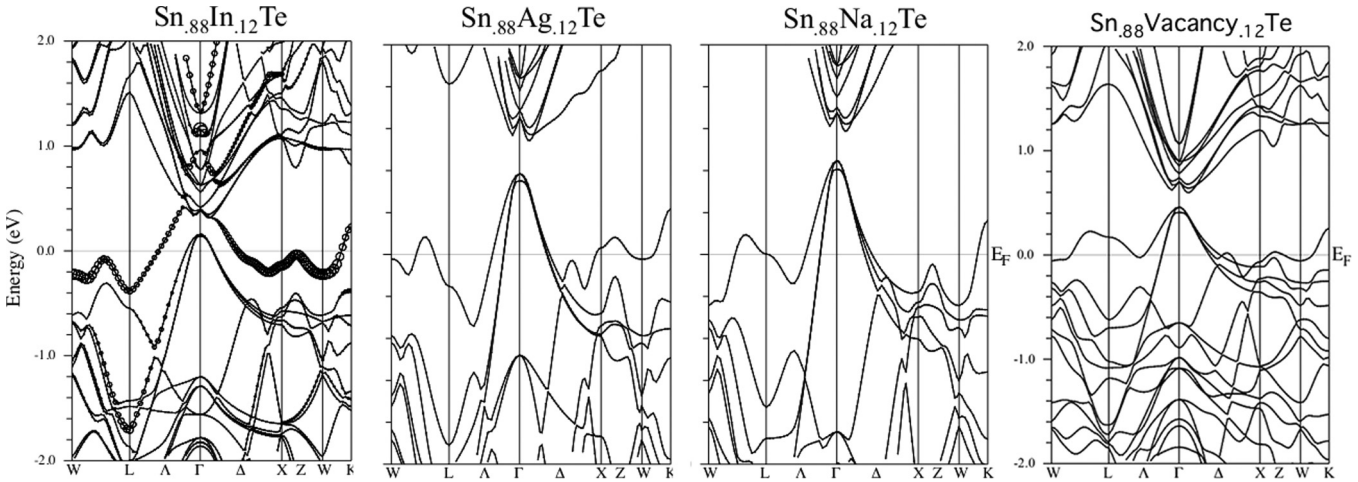

FIG. 6. Calculated electronic band structure for 12% In, Ag, and Na and vacancy doped SnTe. The resonant band at E_F can be observed only in the In doped case.

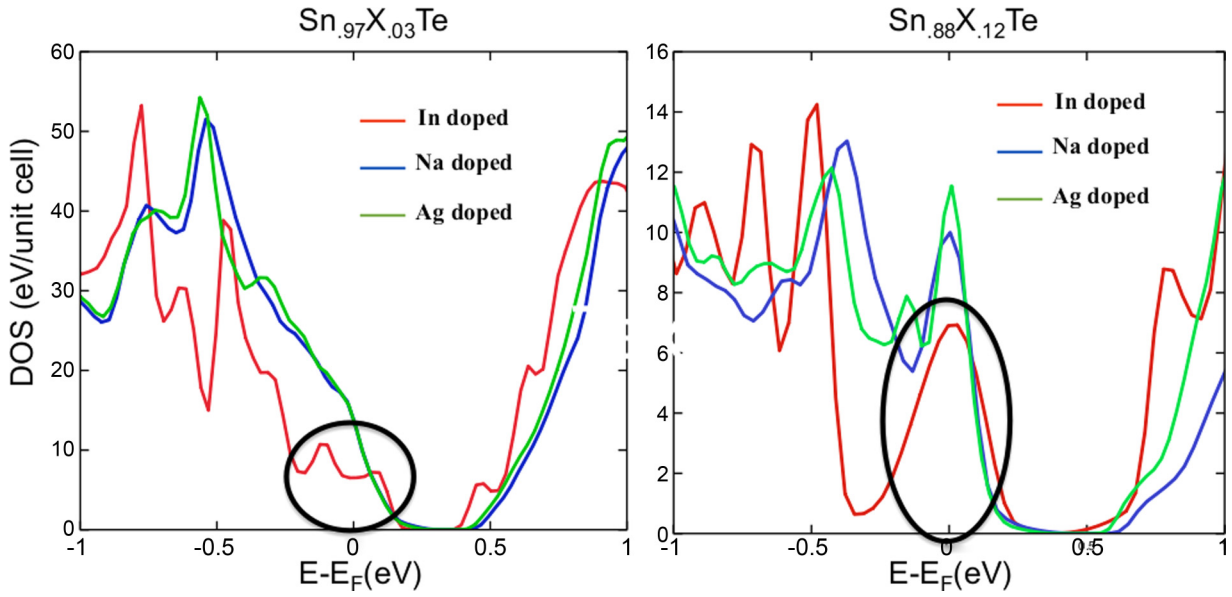

FIG. 7. Density of states as a function of E-E_F for (a) 3% and (b) 12% In, Ag, and Na doped SnTe systems. Vacancy doping yields a DOS that is very similar to that seen for Ag and Na doping, with vacancies being a two-hole dopant rather than a single-hole dopant.

if In were also to occupy an interstitial tetrahedral site rather than replacing an Sn atom, it would act as an *n*-type dopant while still inducing the same in-gap 5*s* state as seen in the previously discussed calculations. This calculation was part of our motivation for the detailed crystallographic study we performed, which showed that In in tetrahedral interstitial sites cannot be found in (Sn,In)Te [37].

Finally, we note that In has been used as dopant to achieve very high resistivities in $Pb_{1-x}Sn_xTe$ [38]. This is consistent with the picture of indium forming an in-gap state. At very low concentrations, this state would be relatively localized and would pin the Fermi energy to the gap, acting as a carrier concentration buffer, much like Sn does in $Sn:Bi_2Te_2Se$ [39–41].

V. CONCLUSION

Our study of a broad range of compositions in the superconducting $Sn_{1-x}In_xTe$ system shows that indium doped SnTe cannot be thought of as a simple hole doped semiconductor over its full superconducting composition range. The nature of the superconductivity and the carrier type change as a function of indium doping, going from overall *p* type to overall *n* type and from a weakly coupled to a strongly coupled superconductor. Furthermore, our DFT calculations show that the dopant In 5*s* states are present at the Fermi level and therefore affect the electronic properties. In recent years, In-doped SnTe has been studied as a superconducting doped topological crystalline insulator; our work indicates that the nature and influence of the In 5*s* states should be considered in such studies. Future work, for example, by spectroscopic techniques, would be of interest to elucidate further the composition-dependent nature of In in SnTe. Finally, the fact that as a function of dopant concentration such a nominally simple system can show both weakly and strongly coupled superconductors, with different dominant carrier types, also suggests that $Sn_{1-x}In_xTe$ is worthy of further investigation.

ACKNOWLEDGMENTS

The materials synthesis and physical property characterization of this superconductor were supported by the Department of Energy, division of basic energy sciences, Grant No. DE-FG02-98ER45706. The single crystal structure determination was supported by the Gordon and Betty Moore Foundation, EPiQS initiative, Grant No. GBMF4412, and the electronic structure calculations were supported by the ARO MURI on topological Insulators, Grant No. W911NF-12-1-0461.

[1] Y. Tanaka, Zhi Ren, T. Sato, K. Nakayama, S. Souma, T. Takahashi, Kouji Segawa, and Yoichi Ando, Nat. Phys. **8**, 800 (2012).
[2] Timothy H. Hsieh, Hsin Lin, Junwei Liu, Wenhui Duan, Arun Bansil, and Liang Fu, Nat. Commun. **3**, 982 (2012).
[3] Y. J. Uemura, G. M. Luke, B. J. Sternlieb, J. H. Brewer, J. F. Carolan *et al.*, Phys. Rev. Lett. **62**, 2317 (1989).
[4] Y. Shimakawa, Y. Kubo, T. Manako, and H. Igarashi, Phys. Rev. B **40**, 11400 (1989).
[5] P. Mandal, A. Poddar, and B. Ghosh, Phys. Rev. B **43**, 13102 (1991).
[6] T. Yildirim, L. Barbedette, J. E. Fischer, C. L. Lin, J. Robert, P. Petit, and T. T. M. Palstra, Phys. Rev. Lett. **77**, 167 (1996).
[7] Fedor F. Balakirev, Jonathan B. Betts, Albert Migliori, S. Ono, Yoichi Ando, and Gregory S. Boebinger, Nature (London) **424**, 912 (2003).
[8] Philip. B. Allen and Marvin L. Cohen, Phys. Rev. **177**, 704 (1969).

[9] A. S. Erickson, J. H. Chu, M. F. Toney, T. H. Geballe, and I. R. Fisher, Phys. Rev. B **79**, 024520 (2009).
[10] R. D. Zhong, J. A. Schneeloch, X. Y. Shi, Z. J. Xu, C. Zhang, J. M. Tranquada, Q. Li, and G. D. Gu, Phys. Rev. B **88**, 020505(R) (2013).
[11] Mario Novak, Satoshi Sasaki, Markus Kriener, Kouji Segawa, and Yoichi Ando, Phys. Rev. B **88**, 140502(R) (2013).
[12] Qian Zhang, Bolin Liao, Yucheng Lan, Kevin Lukas, Weishu Liu, Keivan Esfarjani, Cyril Opeil, David Broido, Gang Chen, and Zhifeng Ren, Proc. Natl. Acad. Sci. **110**, 13261 (2013).
[13] G. S. Bushmarina and I. A. Drabkin, and D. V. Mashovets, R. V. Parfeniev, D. V. Shamshur, and M. A. Shachov, Physica B: Condens. Matter **169**, 687 (1991).
[14] Joseph P. Heremans, Bartlomiej Wiendlocha, and Audrey M. Chamoire, Energy Environ. Sci. **5**, 5510 (2012).
[15] Y. Matsushita, P. A. Wianecki, A. T. Sommer, T. H. Geballe, and I. R. Fisher, Phys. Rev. B **74**, 134512 (2006).
[16] L. Lutterotti, S. Matthies, H. R. Wenk, A. S. Schultz, and J. W. Richardson Jr., J. Appl. Phys. **81**, 594 (1997).
[17] See Supplemental Material at http://link.aps.org/supplemental/10.1103/PhysRevB.93.024520 for detail single crystal structure analysis were performed to verify the rock-salt crystal structure of highly In doped SnTe. All of the atoms were found by direct methods to be located on standard NaCl structure positions. The crystal structure refinement and atomic parameters are given in Tables S1 and S2. The agreement between model and data is excellent, with very small electron density residuals.
[18] P. Blaha, K. Schwarz, G. Madsen, D. Kvasnicka, and J. Luitz, *WIEN2k, An Augmented Plane Wave + Local Orbitals Program for calculating Crystal Properties* (Technische Universitat Wien, Austria, 2001).
[19] D. J. Singh, L. Nordstrom, *Planewaves, Pseudopotentials, and the LAPW Method*, 2nd ed. (Springer, New York, 1996).
[20] G. K. H. Madsen, P. Blaha, K. Schwarz, E. Sjostedt, L. Nordstrom, Phys. Rev. B **64**, 195134 (2001).
[21] E. Sjostedt, L. Nordstrom, D. J. Singh, Solid State Commun. **114**, 15 (2000).
[22] J. P. Perdew, K. Burke, and M. Ernzerhof, Phys. Rev. Lett. **77**, 3865 (1996).
[23] M. Tinkham, *Introduction to Superconductivity*, 2nd ed. (McGraw Hill, New York, 1975).
[24] A. B. Karki, Y. M. Xiong, N. Haldolaarachchige, W. A. Phelan, Julia Y. Chan, S. Stadler, I. Vekhter, P. W. Adams, and D. P. Young, Phys. Rev. B **83**, 144525 (2011).
[25] Neel Haldolaarachchige, Quinn Gibson, Jason Krizan, and R. J. Cava, Phys. Rev. B **89**, 104520 (2014).
[26] Neel Haldolaarachchige, S. K. Kushwaha, Quinn Gibson, and R. J. Cava, Supercond. Sci. Technol. **27**, 105001 (2014).
[27] Neel Haldolaarachchige, Quinn Gibson, Leslie M. Schoop, Huixia Luo, and R. J. Cava, J. Phys.: Condens. Matter **27**, 185701 (2015).
[28] G. Balakrishnan, L. Bawden, S. Cavendish, and M. R. Lees, Phys. Rev. B **87**, 140507(R) (2013).
[29] M. Saghir, J. A. T. Barker, G. Balakrishnan, A. D. Hillier, and M. R. Lees, Phys. Rev. B **90**, 064508 (2014).
[30] N. R. Werthamer, E. Helfand, and P. C. Hohenberg, Phys. Rev. **147**, 295 (1966).
[31] A. M. Clogston, Phys. Rev. Lett. **9**, 266 (1962).
[32] H. Padamsee, J. E. Neighbor, and C. A. Shiffman, J. Low Temp. Phys. **12**, 387 (1973).
[33] A. S. Erickson, N. P. Breznay, E. A. Nowadnick, T. H. Geballe, and I. R. Fisher, Phys. Rev. B **81**, 134521 (2010).
[34] W. L. McMillan, Phys. Rev. **167**, 331 (1968).
[35] *Handbook of Superconductivity*, edited by C. P. Poole Jr. (Academic Press, New York, 1999), Chap. 9, Sec. G, p. 478.
[36] R. J. Cava, B. Batlogg, J. J. Krajewski, R. Farrow, L. W. Rupp Jr, A. E. White, K. Short, W. F. Peck, and T. Kometani, Nature (London) **332**, 814 (1988).
[37] Charles Kittel, *Introduction to Solid State Physics*, 7th ed. (John Wiley and Sons, Inc., New York, 1996).
[38] Ruidan Zhong, Xugang He, J. A. Schneeloch, Cheng Zhang, Tiansheng Liu, I. Pletikosi, T. Yilmaz, B. Sinkovic, Qiang Li, Wei Ku, T. Valla, J. M. Tranquada, and Genda Gu, Phys. Rev. B **91**, 195321 (2015).
[39] Craig S. Lent, Marshall A. Bowen, Robert S. Allgaier, John D. Dow, Otto F. Sankey, and Eliza S. Ho, Solid State Commun. **61**, 83 (1987).
[40] S. K. Kushwaha, Q. D. Gibson, J. Xiong, I. Pletikosic, A. P. Weber, A. V. Fedorov, N. P. Ong, T. Valla, and R. J. Cava, J. Appl. Phys. **115**, 143708 (2014).
[41] Zhi Ren, A. A. Taskin, Satoshi Sasaki, Kouji Segawa, and Yoichi Ando, Phys. Rev. B **85**, 155301 (2012).